Tellus (1994), 46A, 160–177
Printed in Belgium – all rights reserved

TELLUS
ISSN 0280–6495

Tidal averaging and models for anisotropic dispersion in coastal waters

By J. M. DE KOK, *Rijkswaterstaat, Tidal Waters Division, P.O. Box 20907, 2500 EX, The Hague, The Netherlands*

(Manuscript received 4 November 1992; in final form 19 May 1993)

ABSTRACT

Several methods for the computation of long-term approximate solutions of the advection-diffusion equation in tidal waters are discussed. The time step used is a tidal period and the effect of tidal fluctuation is represented by a space-varying diffusion tensor. Further, a new method is presented that allows for more complicated dispersion patterns than can be obtained by the anisotropic diffusion operator. The method is applied to the Dutch Coastal waters, where horizontal and vertical density gradients cause anisotropic and irregular dispersion. Numerical results are compared with a solution, computed with small timesteps and tidal velocities.

1. Introduction

Dealing with the long-term condition of a tidal water system, subject to different inputs from different sources, a set of advection-diffusion equations has to be solved, containing production and decay terms, representing physical, chemical and biological processes. Many input parameters vary on time scales larger than the main tidal period, and often the production and decay terms vary slowly as well.

When there is no back-coupling with the dynamics of the sea water needed, (excluding salinity and temparature), the computational procedure is often as follows: one or more representative tidal periods are run with a hydrodynamical model, (with or without baroclinic pressure terms), and the vertically integrated velocities are averaged in time. The resulting Eulerian residual transport velocities are used in advection-diffusion equations with tidally averaged concentrations as unknown variables, and with a 2-D isotropic diffusion coefficient, calibrated with available salinity data. The time step size for numerical solution can be large, possibly equal to the tidal period. The computational effort is relatively small.

Because residual velocities are generally an order smaller than tidal velocities, cell Peclet numbers and related numerical inaccuracies are smaller as well.

Time-independent solutions can also be computed as a representation of the long-term situation, using spatially varying diffusion coefficients where necessary (de Ruijter et al., 1987). When the horizontal mesh width is larger than the tidal excursion, there will be no large difference between tidally averaged and instantaneous concentration values on the grid. The latter vary little with tide, and the error caused by time averaging of the advection-diffusion equation is unimportant.

Even in these cases, however, a uniform isotropic diffusion is not sufficient, especially in shallow coastal regions with large fresh water outflows from rivers, as is the case in the Dutch coastal waters (Fig. 1). Large residual vertical velocity shear, and small vertical eddy diffusivities, due to stratification of the water column (van der Giessen et al., 1990), combined with very oblong, almost flat tidal ellipses, cause a very large residual dispersion parallel to the coast, and a relatively small one in the normal direction.

This is also the case in very shallow near-shore zones, where vertical shear of tidal velocities is high, acting together with a large bottom generated vertical eddy diffusivity.

In two-dimensional models, an anisotropic space-dependent diffusion operator can be useful, but it complicates a finite difference scheme by the appearance of spatial cross derivatives, which have to be discretised implicitly for stability reasons. The diffusion operator has to represent also the effects of "subgrid-scale" 2-D turbulence, present in nature, but not represented in the velocity field (Uittenbogaard, 1992). A part of this turbulence is associated with subgrid-scale bottom topography and contributes to non linear dispersion (Abraham and Gerritsen, 1990).

The dispersion related to larger-scale turbulence is represented in the model by the interaction of advection, velocity shear and sub-grid-scale diffusion.

In an eddy-resolving model, in general with mesh widths many times smaller than the tidal excursion, and in shallow water, 2-D subgrid-scale diffusion is much smaller then 2-D dispersion caused by vertical shear. In deeper parts of the sea, from 25 m on, it becomes relatively more important (Zimmerman, 1986).

Horizontal velocity shear also causes anisotropy of the dispersion. In an eddy resolving model this shear is represented on the grid for the most important part, and the anisotropy is reproduced by the model. Tidally averaged models, however, include only the effect of residual velocity shear, and an anisotropic diffusion tensor is needed to simulate the tidal shear effects. The use of Lagrangian or semi-Lagrangian methods for advection and diffusion makes it possible to use large time steps and anisotropic diffusion, without need for the time consuming solution of huge linear systems. This makes it worthwhile to compute space-dependent diffusion tensors for use in so-called "tidally averaged" or "tidally integrated" Lagrangian models. These models are a very efficient tool in the assessment of the long term behaviour of tidal water systems. In this paper, we will discuss several of these methods and compare their numerical accuracy.

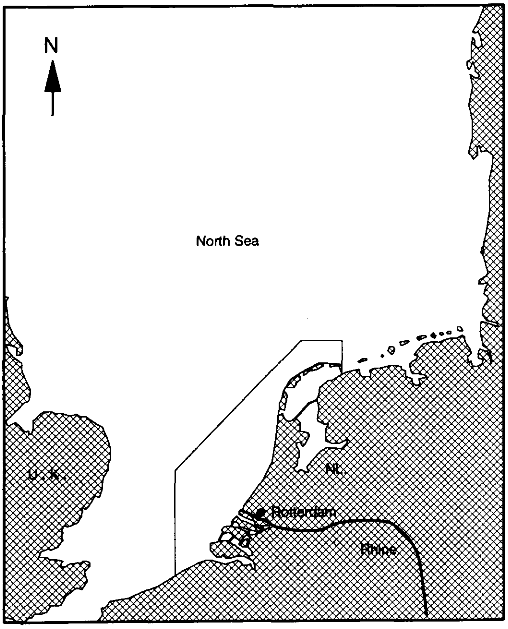

Fig. 1. Southern North Sea with boundaries of the coastal model.

In Sections 2, 3, several methods to compute space dependent two-dimensional diffusion tensors from 2-D tidal velocity fields are described. In order to obtain a good representation of the spatial variation of the important effect of vertical velocity shear, one of these methods is extended with three dimensional information (Section 4).

In Section 5, a new method for tidally-integrated transport computations is presented, based upon superposition of dispersion patterns computed with tidal fluctuation. In Section 6, computational results are compared with the most accurate solution at hand; a run with tidal velocities and two layers. Furthermore, a comparison is made with the standard solution, that is a 2-D run with Eulerian residual transport velocities and uniform isotropic diffusion, and also with a "small cloud" method, described in Section 3.

All computations have been done on an eddy resolving grid ($\Delta x = 1600$ m), representing the Dutch coastal zone, including the part where the Rhine plume induces stratification and baroclinic eddies (Fig. 1).

2. Time averaging of the advection-diffusion equation

In this section, the time averaging in Eulerian and Lagrangian coordinate frames will be discussed. We consider the two-dimensional advection-diffusion equation, without source and sink terms and with constant water depth. $\boldsymbol{u}$ and $\boldsymbol{K}$ are known:

$$\frac{\partial C}{\partial t} + \boldsymbol{u}^{\mathrm{T}} \nabla C = \nabla^{\mathrm{T}} \boldsymbol{K} \nabla C.$$

$C(\boldsymbol{x}, t)$ = depth averaged concentration

$$\boldsymbol{K}(\boldsymbol{x}, t) = \begin{pmatrix} k_{11} & k_{12} \\ k_{12} & k_{22} \end{pmatrix}_{(\boldsymbol{x}, t)}$$

diffusion tensor

$\boldsymbol{u}(\boldsymbol{x}, t) = (u_1(\boldsymbol{x}, t), u_2(\boldsymbol{x}, t))^{\mathrm{T}}$

= velocity vector (depth averaged)

$\boldsymbol{x} = (x_1, x_2)^{\mathrm{T}} = (x, y)^{\mathrm{T}}$

horizontal Cartesian coordinates

$$\nabla C = \left(\frac{\partial C}{\partial x}, \frac{\partial C}{\partial y}\right)^{\mathrm{T}}$$

concentration gradient

$$\nabla^{\mathrm{T}} \boldsymbol{f} = \frac{\partial f_1}{\partial x} + \frac{\partial f_2}{\partial y},$$

divergence of $\boldsymbol{f}$

$$\nabla \boldsymbol{f}^{\mathrm{T}} = \begin{pmatrix} \dfrac{\partial f_1}{\partial x} & \dfrac{\partial f_2}{\partial x} \\ \dfrac{\partial f_1}{\partial y} & \dfrac{\partial f_2}{\partial y} \end{pmatrix}$$

$(\ )^{\mathrm{T}} = (\ )$ transposed

t = time (1)

Eulerian time averaging of the advection-diffusion equation over a tidal period T gives:

$$\overline{\frac{\partial C}{\partial t}} + \overline{\boldsymbol{u}^{\mathrm{T}} \nabla C} = \overline{\nabla^{\mathrm{T}} \boldsymbol{K} \nabla C},$$

$$\overline{\frac{\partial C}{\partial t}} = \frac{1}{T} \int_0^T \frac{\partial C}{\partial t} \, \mathrm{d}t = \frac{C_{\mathrm{T}} - C_0}{T},$$

$$\overline{\boldsymbol{u}^{\mathrm{T}} \nabla C} = \bar{\boldsymbol{u}}^{\mathrm{T}} \nabla \bar{C} + \overline{\boldsymbol{u}'^{\mathrm{T}} \nabla C'}$$

$$\approx \bar{\boldsymbol{u}}^{\mathrm{T}} \nabla \bar{C} + D_1 \nabla^{\mathrm{T}} \nabla \bar{C},$$

$$\overline{\nabla^{\mathrm{T}} \boldsymbol{K} \nabla C} = \nabla^{\mathrm{T}} \bar{\boldsymbol{K}} \nabla^{\mathrm{T}} \bar{C} + \nabla^{\mathrm{T}} \overline{\boldsymbol{K}' \nabla C'}$$

$$\approx \nabla^{\mathrm{T}} \bar{\boldsymbol{K}} \nabla \bar{C} + D_2 \nabla^{\mathrm{T}} \nabla \bar{C},$$

$$\bar{\boldsymbol{u}}(\boldsymbol{x}, t) = \frac{1}{T} \int_{t - T/2}^{t + T/2} \boldsymbol{u}(\boldsymbol{x}, \tau) \, \mathrm{d}\tau$$

residual velocity

$\boldsymbol{u}'(\boldsymbol{x}, t) = \boldsymbol{u}(\boldsymbol{x}, t) - \bar{\boldsymbol{u}}(\boldsymbol{x}, t)$

tidal fluctuation

$f_{\mathrm{T}} = f(\boldsymbol{x}, t)$ at time T

T = tidal period (2)

D_1 and D_2 are extra isotropic diffusion coefficients, representing "tidal mixing" depending on topography, flow structure etc., but also on C'. This tidal mixing can be seen as the result of the product terms with primes and their interaction with each other. When ∇C is important over the tidal excursion area, the product terms with $\boldsymbol{u}'$ and $\boldsymbol{K}'$ are as well. The diffusion coefficients $D_{1,2}$ can not be determined in advance from the flow data, but have to be adjusted experimentally.

When $\nabla \bar{C}$ is time discretized by $\frac{1}{2} \nabla (C_0 + C_{\mathrm{T}})$, the solution of the averaged equation results in instantaneous concentration values at a fixed tidal phase. The time derivative is the average rate of change of the instantaneous concentration values, but it can also be interpreted as the rate of change of the time averaged values $\partial \bar{C} / \partial t$. In this way $\bar{C}$ is the only unknown variable in eq. (2), and the solution has to be interpreted as a tidal mean.

Eq. (1) can be transformed to a moving frame in which the advection term is reduced.

Officer and Lynch (1981) transformed the x-coordinate into a salinity-coordinate (monotone in x), in a one-dimensional estuary, and eliminated in this way the entire advection term. Cheng and Casulli (1982), and Zimmerman (1979) describe the long term transport in terms of Lagrangian residual velocities. Dortch et al. (1992) use first order mass conserving Lagrangian residuals in a 3-D Lagrangian residual transport equation.

Krol (1990) and Heemink (1993) transformed the two-dimensional equation in a Lagrangian frame with respect to the fluctuating part of the Lagrangian velocities. (These lead to closed trajectories). The remaining part belongs to the Lagrangian residual velocity field, and the resulting advection term relates to it. The diffusion term is transformed too, as a result of distortion of the frame. The transformed equations are averaged in time. Within the Lagrangian frame the concentrations are not subject to tidal fluctuation as it is the case in an Eulerian frame. There remains, however, a fluctuation due to diffusion and possible decay terms. The transformed residual velocities and diffusion tensors are not constant in time. This causes fluctuating cross terms which are much smaller however than in case of the Eulerian averaging procedure.

The tidally averaged Lagrangian velocities and diffusion tensors vary in space. Krol and Heemink compute them in a separate run with tidal velocities. From each grid cell a particle is released and followed during a tidal period. The transformed diffusion tensor is computed along the trajectory at small time intervals and time averaged afterwards. The resulting particle displacement determines the residual Lagrangian velocity. The phase of the tidal cycle at the time of release of the particles has effect on the results. It has to be chosen in a way, that the result is close to the average.

3. Small cloud computation

In this section, an alternative treatment of Lagrangian tidal averaging will be presented. Instead of the transformation to a fully distorting Lagrangian frame, we do a local transformation to a rigid frame that moves with a uniform speed. During a tidal cycle we follow a small cloud of mass that is present within a grid cell at $t=0$. The second mass moments and cross moments of that mass change due to the distortion of the cloud by velocity gradients and due to diffusion.

The mass moments are defined as follows:

Mass: $M=\int^{\text{cell}}\int C(\boldsymbol{x}, t)\,\mathrm{d}\boldsymbol{x}$,

first mass moment:

$$M\mu_i=\int^{\text{cell}}\int x_i C(\boldsymbol{x}, t)\,\mathrm{d}\boldsymbol{x},$$

second mass moment:

$$M\sigma_{ij}=\int^{\text{cell}}\int x_i x_j C(\boldsymbol{x}, t)\,\mathrm{d}\boldsymbol{x}-M\mu_i\mu_j,$$

covariance matrix:

$$\boldsymbol{\Sigma}_t=\begin{pmatrix}\sigma_{11} & \sigma_{12}\\ \sigma_{12} & \sigma_{22}\end{pmatrix}_{(t)}. \tag{3}$$

At small time intervals, the actual covariance matrix $\boldsymbol{\Sigma}_t$ with respect to the second mass moments can be computed. (Several formulas for this will be discussed in this section). After one tidal cycle, this matrix has value $\boldsymbol{\Sigma}_{\mathrm{T}}$. When $\boldsymbol{\Sigma}_0$ is the initial value, and $(\boldsymbol{\Sigma}_{\mathrm{T}}-\boldsymbol{\Sigma}_0)=2\boldsymbol{K}^*T$, then the solution of the equation (Fischer et al., 1979)

$$\frac{\partial C}{\partial t}=\boldsymbol{K}^*\,\nabla^{\mathrm{T}}\,\nabla C \tag{4}$$

defined in a rigid frame, moving with the speed of the centre of mass, approximates the solution of eq. (2) (neglecting among others third and higher mass moments, see Appendix B). Now for each grid cell, the residual Lagrangian displacement vector $\boldsymbol{d}$, and the residual diffusion tensor $\boldsymbol{K}^*$ are computed and stored.

The tidally averaged (or better "integrated") computation can then be done with a Lagrangian method that can represent anisotropic diffusion, such as a random walk method, a "small cloud" computation (Holly and Usseglio-Polatera, 1984) or an extended second moment method (de Kok, 1992).

These methods consist of the following steps. At $t=0$ for each grid cell, the 1st and 2nd moments of the mass present within that cell are computed. Then the centre of mass is displaced along the (interpolated) Lagrangian residual displacement vector $\boldsymbol{d}_{\mathrm{c}}$, and eq. (4) (applied to the cell mass only), is integrated over T. This leads to a change of the covariance matrix with $2\boldsymbol{K}^*T$. After this the mass can be redistributed over the grid using the covariance matrix $\boldsymbol{\Sigma}_{\mathrm{T}}$, assuming an appropriate shape function (Fig. 2). Redistribution algorithms are described in de Kok (1992, 1993).

During the redistribution step, the mass is split up, and divided over the grid cells it occupies. A grid cell can then contain contributions, originating from different cells, which are superposed. The covariance matrix of the composite can be computed according to eq. (3).

For the computation of $\boldsymbol{\Sigma}_t$ during the run with tidal resolution, several methods exist. According to Sykes and Henn (1992), $\boldsymbol{\Sigma}_t$ develops according to:

$$\frac{\mathrm{d}\sigma_{ij}}{\mathrm{d}t}=\sum_{l=1,2}\left\{\sigma_{il}\frac{\partial u_j}{\partial x_l}+\sigma_{jl}\frac{\partial u_i}{\partial x_l}\right\}+2k_{ij} \tag{5}$$

with k_{ij} the instantaneous diffusion tensor. This result can be obtained by time differentiation of the

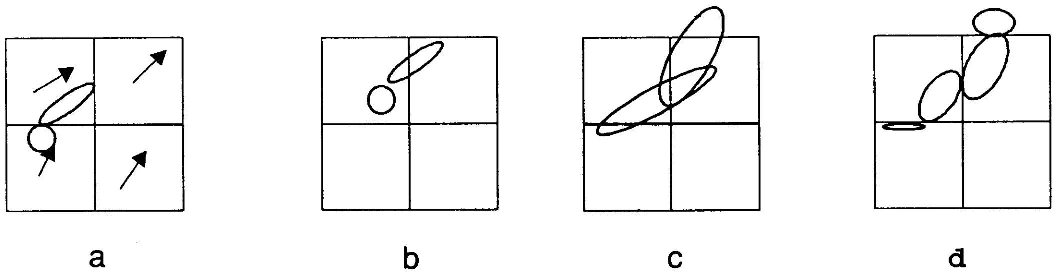

Fig. 2. Advection, diffusion and redistribution steps of a tidally integrated dispersion computation, applied to two "small clouds" with ellipsoidal shapefunctions: (a) initial; (b) after advection step; (c) after anisotropic diffusion step; (d) after redistribution over the occupied grid cells.

expressions for first and second mass moments in the Cartesian frame and by substitution of the advection-diffusion equation for divergence free flows. The time varying velocity gradients are assumed constant throughout the cloud.

In waters with depth gradients, the depth averaged velocities are not divergence free (see Fig. 3b). It is then useful to integrate over the depth H.

Eq. (1) becomes:

$$\frac{\partial HC}{\partial t}+\nabla^{\mathrm{T}}(\boldsymbol{u}HC)=\nabla^{\mathrm{T}}H\boldsymbol{K}\nabla C, \tag{6}$$

and can be written as:

$$\frac{\partial HC}{\partial t}+\nabla^{\mathrm{T}}(\boldsymbol{u}^{\mathrm{d}}HC)=\nabla^{\mathrm{T}}\boldsymbol{K}\nabla(HC),$$
$$\boldsymbol{u}^{\mathrm{d}}=\boldsymbol{u}+\frac{\boldsymbol{K}\nabla H}{H}. \tag{7}$$

The following alternative expression for eq. (5) is derived for this case in Appendix C:

$$\Sigma(t+\Delta t)=\boldsymbol{P}_x^{\mathrm{T}}(t)\,\Sigma(t)\,\boldsymbol{P}_x(t)+2\boldsymbol{K}(t)\,\Delta t. \tag{8}$$

$\boldsymbol{P}_x=\boldsymbol{I}+\nabla\boldsymbol{d}^{\mathrm{T}}$, with $\boldsymbol{d}$ the Lagrangian displacement during Δt connected with $\boldsymbol{u}^{\mathrm{d}}$. This expression does not contain time derivatives, in contrast to eq. (5). The time discretisation error is mainly in the approximation of $\boldsymbol{P}_x$.

Ridderinkhof (1990) uses a particle method to compute the resulting covariance matrix. Particles are released from several positions, close to each other at $t=0$ and advected during a run with tide. At $t=T$, the covariance matrix is computed from the particle positions by

$$\sigma_{ij}^2=\frac{1}{N}\sum_{k=1}^{N}x_i(k)\,x_j(k)-\mu_i\mu_j,$$
$$\mu_i=\frac{1}{N}\sum_{k=1}^{N}x_i(k). \tag{9}$$

N is the number of particles.

The difference with the former mentioned methods is that during the computation with tide, no higher order moments are neglected. Only at $t=T$ is an approximation made by the representation of the cloud by first and second moments.

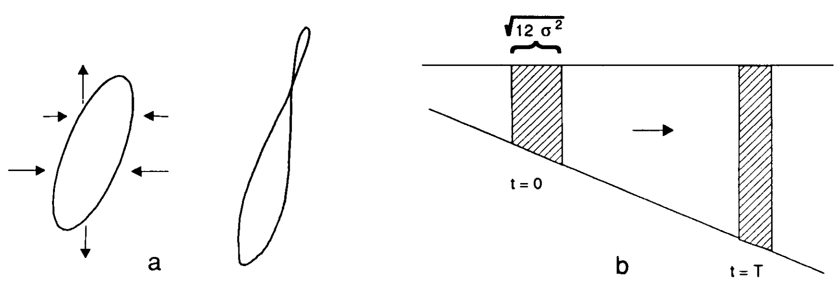

Fig. 3. (a) Folding of patch. (b) Decrease of variance due to non divergence free vertically averaged velocities.

Computations with vertically averaged velocity fields, computed for the Dutch coastal zone, showed no large differences between the methods of Krol and Heemink and of Sykes and Henn. The method following eq. (8) was more robust, in the sense that det $|\Sigma|$, was always positive. In the method of Sykes and Henn, det $|\Sigma|$ becomes negative once in a while, as a result of the "folding" of a patch (see Fig. 3a), when time steps are too large. This leads to the computation of negative variances.

The method of Ridderinkhof was slightly modified here, in the sense that diffusion was added. The method resulted in residual diffusivities that were on the average 20% higher than those, obtained by the other methods.

$$K^{\mathrm{A}} = \frac{1}{2T}(\{\sqrt{\sigma_{11}^2\sigma_{22}^2 - \sigma_{12}^2}\}_{(\mathrm{T})} - \sigma_0^2) \qquad (10)$$

was taken as a measure for the residual diffusivity. σ_0^2 was the initial variance in both directions. When a patch starts in very shallow water and ends up in much deeper water at $t = T$, then it is possible that K^{A} becomes negative (Fig. 3b). This was very exceptional.

A constant uniform isotropic instantaneous diffusion coefficient of 1 m^2/s was used ($\boldsymbol{K} = \boldsymbol{I}$). Increasing it to 10 m^2/s caused no significant change of the differences between the methods. There was a small difference in 1st mass moments between the results following Ridderinkhof and the others. This was caused by the fact that in the other methods, only the velocity in the centre of mass is responsible for advection, while in the Ridderinkhof method, each particle is advected with a different speed. These do not average out to the speed of the mass centre, when the particles are not all within the same grid cell. In Table 1, Section 4, values of K^{A} are listed, computed with formulae (5) and (8), and with Ridderinkhofs method (modified).

4. Two-dimensional diffusion tensors from 3-D velocity fields

In Section 3, two-dimensional models have been discussed, which inlcude only the effect of horizontal velocity differences. In shallow coastal regions vertical velocity shear is the main horizontal dispersion mechanism for small patches (with areas up to 10^6 m^2). The direction and amount of anisotropy is among others dependent on bottom geometry and shore line. Close to the Dutch coast, tidal ellipses are very flat. The tidal excursion at the surface is 10 to 20 km. Residual surface velocities are 0.05 to 0.2 m/s under average conditions.

In the Dutch coastal zone, outflowing fresh Rhine water causes stratification (Van der Giessen et al., 1990), associated with large horizontal dispersion (see, e.g., Fischer et al., 1979; Okubo, 1967; Chickwendu and Ojiakor, 1985). Under certain circumstances, the Rhine plume is subject to baroclinic instablities wich cause very irregular residual flow patterns.

To include the effects of vertical velocity and concentration gradients, a method for the computation of two-dimensional horizontal residual dispersion tensors is introduced here, that is based on a two-layer approach. Eq. (8) is used to account for horizontal velocity gradients. The computed residual dispersion tensors can be used in a two-dimensional tidally integrated dispersion model as described in Section 3. For the computation of the residual dispersion tensors for every grid cell, a small cloud is followed during a tidal cycle, using tidal velocities (in two layers), generated by a two-layer model, representing most of the horizontal and vertical shear. A mixing length model with damping functions for the reduction of vertical turbulence by salinity stratification was used to compute time and space dependent vertical eddy diffusion coefficients. After release of a column with homogeneous initial concentration at $t = 0$, the developing cloud is represented by two masses M_1 and M_2, with horizontal first mass moments $M_1\boldsymbol{\mu}_1$ and $M_2\boldsymbol{\mu}_2$ and horizontal covariance matrices $\boldsymbol{\Sigma}_1$ and $\boldsymbol{\Sigma}_2$. $M_1 + M_2 = M$. M_1 and M_2 are advected with the velocities $\boldsymbol{u}^{\mathrm{d}}_{1,2}$ in upper and lower layer respectively, and each time step new intermediate values for the first mass moments are approximated by

$$M_i\boldsymbol{\mu}_i' = M_i(\boldsymbol{\mu}_i(t) + \boldsymbol{u}_i^{\mathrm{d}}(t)\,\Delta t), \qquad i = 1, 2.$$

The matrices $\boldsymbol{P}_{xi}$ are computed for both layers, and the new intermediate values for the covariance matrices are

$$\boldsymbol{\Sigma}_i' = \boldsymbol{P}_{xi}^{\mathrm{T}}\boldsymbol{\Sigma}_i\boldsymbol{P}_{xi} + 2\boldsymbol{K}_i\,\Delta t.$$

Then the vertical advective and diffusive transport of mass F_1 from layer 1 to layer 2 is computed in $\boldsymbol{\mu}'_1$ and the mass F_2, transported from layer 2 to layer 1 is computed in $\boldsymbol{\mu}'_2$. The algorithm for computation of the vertical mass transports is described in Appendix A. It is of first order accuracy in time.

At the new time level (in Cartesian coordinates):

$$M_i(t+\Delta t) = M_i(t) - F_i + F_j, \tag{11}$$

$$(M_i\boldsymbol{\mu}_i)_{(t+\Delta t)} = M_i(t)\,\boldsymbol{\mu}'_i - F_i\boldsymbol{\mu}'_i + F_j\boldsymbol{\mu}'_j, \tag{12}$$

$$(M_i(\boldsymbol{\Sigma}_i + \boldsymbol{\mu}_i\boldsymbol{\mu}_i^{\mathrm{T}}))_{(t+\Delta t)} = M_i(t)(\boldsymbol{\Sigma}'_i + \boldsymbol{\mu}'_i\boldsymbol{\mu}_i'^{\mathrm{T}}) - F_i(\boldsymbol{\Sigma}'_i + \boldsymbol{\mu}'_i\boldsymbol{\mu}_i'^{\mathrm{T}}) + F_j(\boldsymbol{\Sigma}'_j + \boldsymbol{\mu}'_j\boldsymbol{\mu}_j'^{\mathrm{T}}). \tag{13}$$

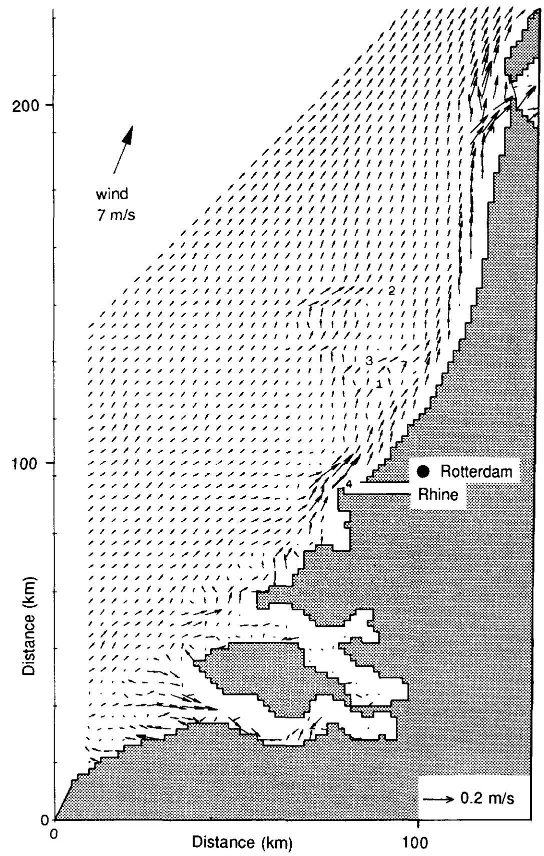

Fig. 4. Lagrangian residual velocities from vertically-averaged values of tidal velocities computed with a two-layer model. This pattern occurred after one week of moderate NE winds and large Rhine outflow. Then the wind veered to SSW. After several days with constant wind, the pattern was almost stable. The numbers indicate the release points of the numerical experiments.

At $t = T$, the mass moments of upper and lower layer are summed to obtain the residual two-dimensional horizontal diffusion tensor $\boldsymbol{K}^* = (\boldsymbol{\Sigma}_{\mathrm{T}} - \boldsymbol{\Sigma}_0)/2T$ and the vertically averaged Lagrangian residual velocity $\boldsymbol{u}^* = (\boldsymbol{\mu}_{\mathrm{T}} - \boldsymbol{\mu}_0)/T$.

$$\boldsymbol{\mu}_{\mathrm{T}}(T) = (M_1(T)\,\boldsymbol{\mu}_1(T) + M_2(T)\,\boldsymbol{\mu}_2(T))/M, \tag{14}$$

$$\boldsymbol{\Sigma}_{\mathrm{T}} = (M_1(T)(\boldsymbol{\Sigma}_1 + \boldsymbol{\mu}_1\boldsymbol{\mu}_1^{\mathrm{T}})_{(\mathrm{T})} + M_2(T)(\boldsymbol{\Sigma}_2 + \boldsymbol{\mu}_2\boldsymbol{\mu}_2^{\mathrm{T}})_{(\mathrm{T})})/M - (\boldsymbol{\mu}\boldsymbol{\mu}^{\mathrm{T}})_{\mathrm{T}} \tag{15}$$

$\boldsymbol{u}^*$ is among others dependent on vertical diffusion and shear. The values of $\boldsymbol{u}^*$ are smoother than those plotted in Fig. 4, showing the Lagrangian means of vertically averaged velocities.

Numerical experiments were done with tidal velocity fields from the two-layer model of the Dutch coastal zone, including stratified areas in the Rhine outflow region, with vertical diffusion coefficients below 10^{-4} m^2/s. In this region, the velocity differences between the layers are most of the time larger than 0.5 m/s and the vertical differences of the residuals are about 0.1 m/s. Depths range from 10–30 m. An instantaneous horizontal diffusion coefficient of 1 m^2/s was used in all transport computations (with tide). $\Delta x = 1600$ m. $\Delta t = 1800$ s.

The used "tidal" velocities were not determined by tide only, but also by varying wind and density structure of the water. They were taken from the last part of a simulated event with large Rhine outflow (4000 m^3/s). After a period of moderate northeasterly winds the wind veered to SSW. A large baroclinic eddy was present in the computed residual velocity field (Fig. 4). A similar pattern can often be observed in satellite images of measured sea surface temperature in the Rhine plume after a period of NE to easterly winds.

Residual diffusion tensors after a point release with $\sigma_0^2 = \Delta x^2/12$ were determined with the following methods:

(a) vertically averaged velocities and formula (5);

(b) vertically averaged velocities and formula (8);

(c) vertically averaged velocities and formula (9);

(d) two-layer velocities and formulae (11–15);

(e) two-layer velocities and formulae (14, 15) applied to the result of a full numerical computation of the two-layer advection-diffusion equation.

In Table 1, the isotropic residual diffusion coefficients K^A, computed following formula (10), are given for several points (see Fig. 4).

The large difference between methods (a), (b), (c), and (d), (e) is due to the fact that in all methods, the same isotropic horizontal instantaneous diffusion coefficient was used. The effect of

Table 1. *Isotropic residual diffusion coefficients K^A in m^2/s (see eq. (10)), computed after one tidal cycle for the different methods*

	Method:				
Location	(a)	(b)	(c)	(d)	(e)
1	1.04	1.05	1.8	20	24
2	1.04	1.04	1.24	2.5	2.5
3	1.13	1.16	16	31	35
4	1.01	1.20	2.5	36	53

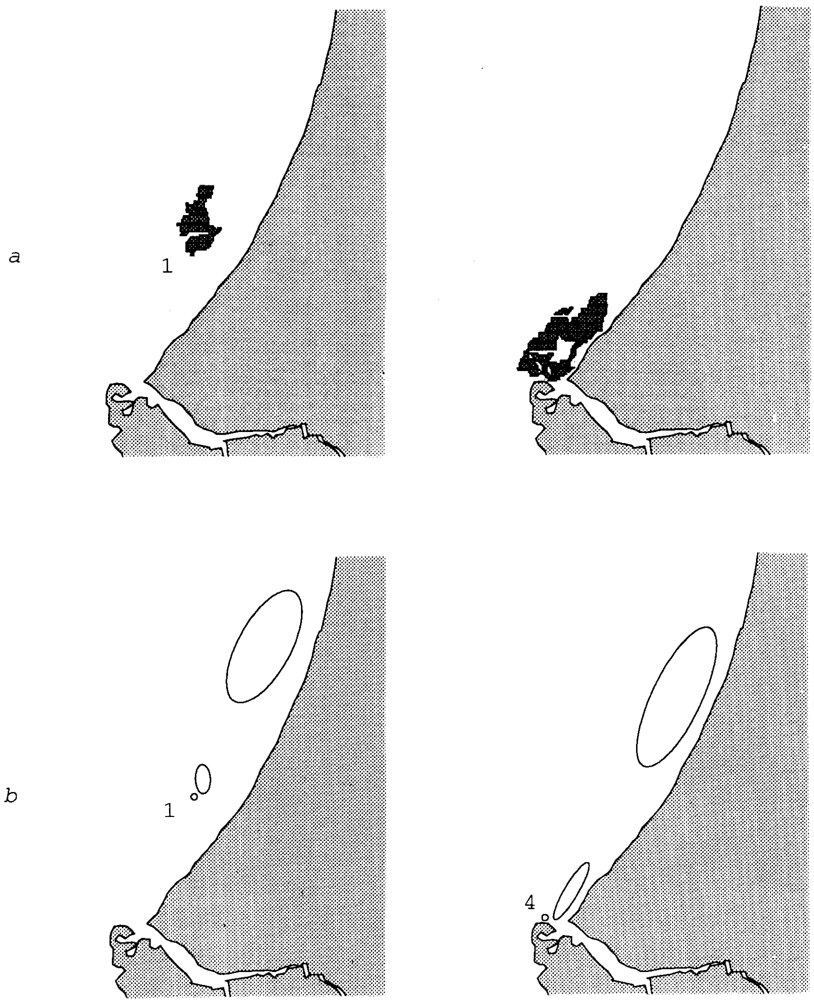

Fig. 5. (a) Dispersion patterns after one tidal cycle of computation (e), for initial locations 1 and 4. (b) Ellipses of covariances of the dispersion patterns after 1 and 10 tidal cycles, for computation (e).

vertical shear was therefore not represented in methods (a), (b), (c).

Release point 2 is located outside the stratified zone. Vertical mixing is larger there, and velocity shear is low, resulting in relatively small horizontal dispersion. Point 3 is located in the baroclinic eddy with large higher order velocity gradients. Higher order mass moments become then important for the residual dispersion, but are ignored in method (a) and (b).

From the results in Table 1, it may be clear, that in a two-dimensional computation of the residual dispersion tensor, an extra instantaneous diffusion coefficient is needed, to include the effect of vertical shear dispersion. This diffusion coefficient is very variable, as a result of local occurrence of stratification.

Fig. 5b shows the ellipses (long and short axes according to eqs. (16) and (17)) belonging to the covariance matrices of the results of computation (e) for locations 1 and 4, at $t=0$, $t=T$ and $t=10T$. Fig. 5a shows the dispersion patterns of computation (e) at $t=T$. All mass is contained within the shaded areas. Fig. 10 shows the result of computation (e) for release point 4 at $t=10T$.

In Fig. 6, values of the residual diffusion coefficients K^{A}, resulting from method (e) at $t=T$ are plotted for all grid points. Around tidal inlets and in the baroclinic eddy north-west of Rotterdam, dispersion is high as a result of irregular 2-D flow patterns. In the stratified part of the Rhine plume and in the shallow near-shore zone, vertical residual shear contributes to high diffusivities. The average of all computed values was 10.2 m^2/s.

Van Dam (1982) reports values of residual diffusion coefficients, based on tracer experiments, of 1 m^2/s for small clouds ($\sigma^2=10^4$ m^2) and of 10 m^2/s for patches of 10^6 m^2 in the Southern

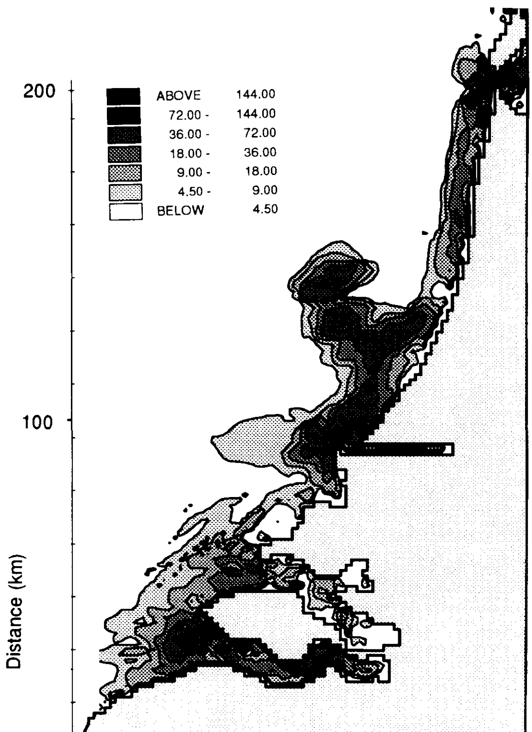

Fig. 6. Isotropic diffusion coefficient values K^{A} (m^2/s) based upon det $|\boldsymbol{K}^*|$, computed with two-layer model.

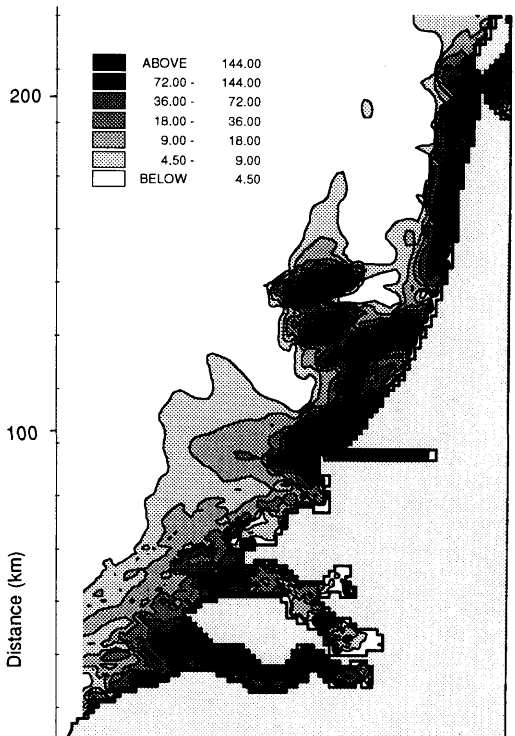

Fig. 7. Values of diffusion coefficient K^{L} (m^2/s) based upon long axis of $\boldsymbol{K}^*$, computed with two-layer model.

North Sea, 60 km off shore. The model gives there values of 4 m^2/s. The effect of subgridscale horizontal turbulence was apparently not represented by the used instantaneous diffusion coefficient of 1 m^2/s.

In Fig. 7, the residual diffusion coefficients along the longitudinal axes of the computed patches are plotted. These are determined according to

$$K^{\mathrm{L}} = \frac{1}{2T}(\lambda_1 - \sigma_0^2),$$
$$\lambda_1 = \tfrac{1}{2}\{\sigma_{11}^2 + \sigma_{22}^2 + \sqrt{(\sigma_{11}^2 - \sigma_{22}^2)^2 + 4\sigma_{12}^2}\}_{(\mathrm{T})}, \tag{16}$$

the largest eigenvalue of $\boldsymbol{\Sigma}_{\mathrm{T}}$.

Very high values (above 500 m^2/s) are found in the vicinity of the outlet of the Rhine, among others due to large residual vertical shear and stratification. Values between 250 and 500 m^2/s are found around the main tidal inlet of the Western Wadden Sea, situated in the north-eastern corner of the model. Ridderinkhof (1990) computed values between 100 and 500 m^2/s with a fine resolution 2-D model for the same inlet. In these regions dispersion patterns are very irregular, with large higher order moments. Values of the anisotropy ratio $K^{\mathrm{L}}/K^{\mathrm{S}}$ are plotted in Fig. 8. K^{S} is computed along the short axis of the dispersion pattern according to

$$K^{\mathrm{S}} = \frac{1}{2T}(\lambda_2 - \sigma_0^2),$$
$$\lambda_2 = \tfrac{1}{2}\{\sigma_{11}^2 + \sigma_{22}^2 - \sqrt{(\sigma_{11}^2 - \sigma_{22}^2)^2 + 4\sigma_{12}^2}\}_{(\mathrm{T})}, \tag{17}$$

the smallest eigenvalue of $\boldsymbol{\Sigma}_{\mathrm{T}}$. Figs. 6, 7 and 8 indicate, that when the residual diffusion is large, it is also very anisotropic.

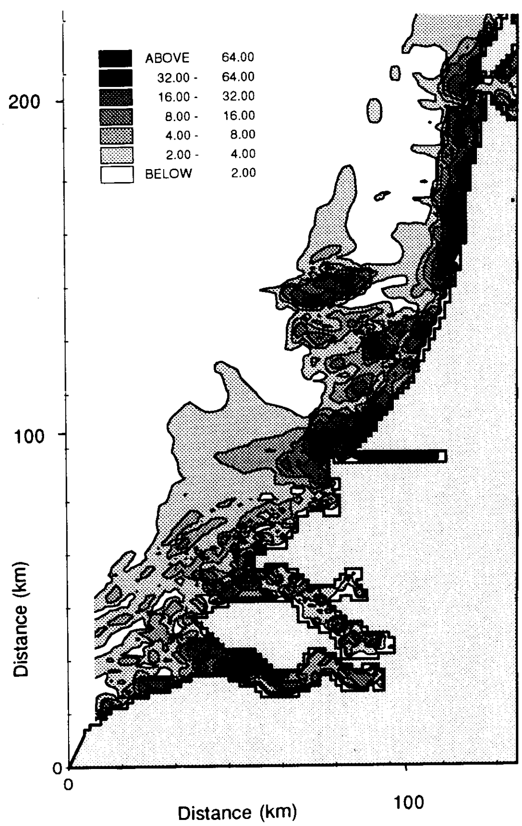

Fig. 8. Values of the anisotropy ratio $K^{\mathrm{L}}/K^{\mathrm{S}}$, computed with two-layer model.

5. Lagrangian superposition methods

In Section 3, a method was described for tidally averaged two-dimensional advection-diffusion computations, based upon the "small cloud" approximation of grid cell masses. The distribution at $t = T$ of a mass M_k, originating at $t = 0$ from a grid cell k is characterised by the position of the centre of mass and the covariance matrix: $(M, \boldsymbol{\mu}, \boldsymbol{\Sigma})_k$. By superposition of contributions of all k and redistribution over the grid, at $t = T$, a new initial situation is computed, in which each grid cell contains at most one small cloud (Fig. 2).

The change of the first two mass moments during one tidal cycle can directly be computed from the Lagrangian residual velocity and the residual dispersion tensor $\boldsymbol{K}^*$. When velocities are periodic (with the tidal period), these quantities are constant in time. They are space dependent and can be computed for every grid cell. This can be done with vertically averaged or with 3-D tidal velocities. Several 2-D methods and a two-layer method were described in the preceding sections. Velocity gradients are assumed the same throughout the cloud.

Greater accuracy can be obtained when the dispersion pattern of a cloud is characterised by more parameters than the first two moments. This necessitates the computation of the resulting cloud at $t = T$ with an accurate Lagrangian method on a grid with mesh size, that is at least several times smaller than the tidal excursion. A cloud covers after a tidal period several grid cells, and is distorted by the influence of higher spatial velocity derivatives.

We used an extended second moment method (de Kok, 1993) for this computation. The method represents small clouds in a very compact way. It is even somewhat compressive in the sense that tails of small Gaussian distributions are suppressed, reducing the number of occupied grid cells (Fig. 9).

The essence of the method is (in two dimensions), that at every time step, the concentration field is not only given by cell averaged concentration values at grid points, but also, for each grid cell, by the first two mass moments and cross moments. These parameters are stored in arrays and advected in a Lagrangian way. The change of the covariance matrix, caused by velocity gradients and diffusion during this advection/diffusion step, can be computed with formula (5) or (8). In a redistribution step (see, e.g., Fig. 2) the mass is remapped on the grid in a way, that as much as possible of the mass, assigned to a certain grid cell, is situated within that cell. During redistribution first and second moments are conserved applying eq. (3).

When we start with a small cloud in a grid cell at $t=0$, we compute, in a run with tidal resolution, the resulting cloud at $t=T$ (see, e.g., Fig. 5a). If this cloud occupies N grid cells, we have at our disposal the values of $((M_j, \boldsymbol{\mu}_j, \boldsymbol{\Sigma}_j),\ j=1, N)$, that is per occupied grid cell j: the cell mass, its centre position and covariance matrix. These $6N$ parameters describe the dispersion pattern of the cloud.

It is also possible to do this run in 3 dimensions or with 2 layers.

In the two-layer case, the vertical advective and diffusive transports can be computed in a separate step (which is described in Appendix A). At $t=T$, the distributions in upper and lower layer are superposed, and the resulting $(M_j, \boldsymbol{\mu}_j, \boldsymbol{\Sigma}_j)$ can be computed per occupied (2-D) cell j, using formulae (14) and (15).

The computation with tide is repeated for each grid cell in the horizontal, starting with an initial unit mass (vertically homogeneous) in that grid cell. This results in a set $(((M_j, \boldsymbol{\mu}_j, \boldsymbol{\Sigma}_j)_k,\ j=1, N_k),\ k=1, G)$ where G is the number of grid cells (horizontal).

One can compute now for all k a "distributed" Lagrangian residual velocity

$$(M_j, \mathbf{u}_j^*)_k,$$

$$(\boldsymbol{u}_j^*)_k = (\boldsymbol{\mu}_j - \boldsymbol{\mu}_0)_k/T, \qquad j=1, N_k,$$

and a distributed residual diffusion tensor:

$$(M_j, \boldsymbol{K}_j^*)_k,$$

$$(\boldsymbol{K}_j^*)_k = (\boldsymbol{\Sigma}_j - \boldsymbol{\Sigma}_0)_k/2T, \qquad j=1, N_k.$$

$$M_k(\boldsymbol{\Sigma} + \boldsymbol{\mu}\boldsymbol{\mu}^{\mathrm{T}})_{Tk} = \sum_{j=1}^{N_k} (M_j\boldsymbol{\Sigma}_j + \boldsymbol{\mu}\boldsymbol{\mu}_j^{\mathrm{T}})_{Tk}$$

$$= M_k(\boldsymbol{\Sigma}_0 + \boldsymbol{\mu}_0\boldsymbol{\mu}_0^{\mathrm{T}})_k + \sum_{j=1}^{N_k} M_j(2\boldsymbol{K}_j^* T + \boldsymbol{d}\boldsymbol{d}_j^{\mathrm{T}})_k,$$

$$\boldsymbol{\mu}_{Tk} = \boldsymbol{\mu}_{0k} + \sum_{j=1}^{N_k} \frac{M_j}{M_k}(\boldsymbol{d}_j)_k, \qquad (\boldsymbol{d}_j)_k = (\boldsymbol{u}_j^*)_k T.$$

$(\boldsymbol{K}_j^*)_k$ and N_k are dependent on $(\boldsymbol{\Sigma}_0)_k$. The most probable $\boldsymbol{\Sigma}$ in large patches is $\boldsymbol{I}\,\Delta x^2/12$. We took this as an initial value to determine the $\boldsymbol{K}_j^*$.

It is possible, but not very efficient to apply the algorithm described in Appendix B, to determine an invariant $\boldsymbol{K}_{\Gamma j}$. $\boldsymbol{K}_j^*$ can then be computed at

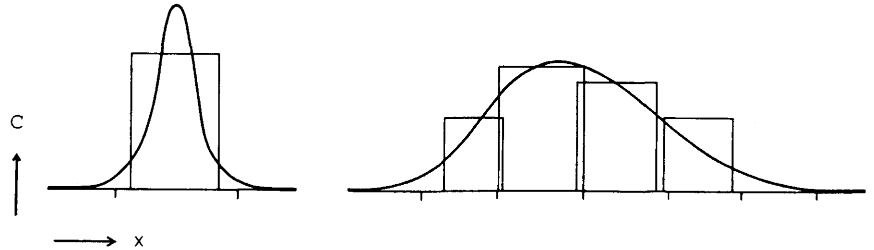

Fig. 9. Discontinuous shape functions conserve mass, 1st and 2nd mass moments in the 2nd moment method.

every timestep in the tidally averaged computation from:

$$K_j^* = K_{\Gamma j} + (\Sigma_d + \Sigma_d^T P_\Gamma)_j / 2T,$$
$$\Sigma_{dj} = \Sigma_{to} \nabla d_j^T,$$
$$P_{\Gamma j} = I + \nabla d_j^T.$$

The distributed residual Lagrangian velocities and diffusion tensors have to be stored, preferably in core. For the Dutch coastal model this required not more than four megabyte.

The tidally averaged computation is similar to that described above for the residual small cloud computation. A time step ($\Delta t = T$) is as follows.

For each grid cell, k, the mass $(M, \mu_t, \Sigma_t)_k$, present in that cell at time t, is divided in N_k masses M_j which are displaced with the residual velocities $(u_j^*)_k$. The related 1st and 2nd (with respect to the centre of mass) mass moments become:

$$(M_j(\mu_t + u_j^* T))_k,$$
$$(M_j(\Sigma_t + 2K_j^* T))_k, \qquad j = 1, N_k.$$

The redistribution step is different from that used in the second moment method, there is no splitting of mass during this step, only superposition. The first mass moment determines to which cell a mass M_j is now assigned. All masses assigned to the same cell are superposed, and their mass moments are summed according to eq. (3). Only when variances become too large, a regular redistribution step is performed. By the superposition there is temporarily lumping of mass. This is not cumulative, because the mass is split up in the next displacement step. The method uses very little computer time and is easy to implement. If K_j^* is determined in a tidal run with $\Sigma_0 = 0$, det $|K_j^*|$ is always positive, if $\Sigma_0 \neq 0$, there is a chance that det $|K_j^*|$ becomes negative. This does not matter, because $2K_j^* T$ is added to covariance matrices, with mostly positive determinants.

Results of numerical experiments did not lose much quality when no second moments were computed at all. Given the large ratio tidal excursion/grid mesh size of the model used, the distribution of the residual velocities u_j^* was apparently computed with sufficient detail, that is, the number N_k was on the average large enough.

6. Comparison, discussion and conclusion

We compare now the results of computations with different methods over ten tidal cycles with the 1600 m Dutch coast model. An initial (vertically homogeneous) cloud with $\sigma_0^2 = \Delta x^2/12$ was released at point 4, in front of the Rhine outlet.

The following methods were used.

(a) 2-layer computation with tide,

$D_{\text{horiz.}} = 1\ \text{m}^2/\text{s}$ (Fig. 10).

(b) Tidally-averaged run with distributed residual velocities, computed with two-layer model. No diffusion tensors used. (Fig. 11).

(c) Tidally-averaged run with Lagrangian residual velocities and residual diffusion tensors (not distributed), computed directly from disper-

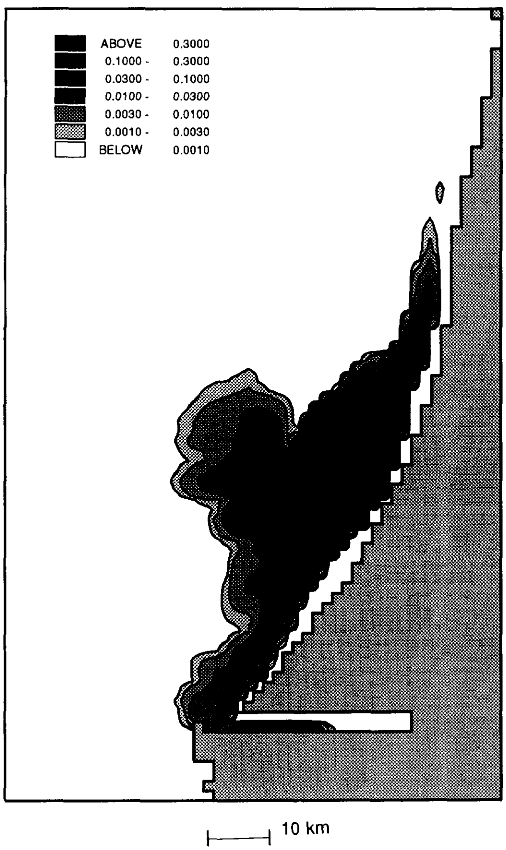

Fig. 10. Dispersion pattern after a point release in point 4. Computation with two layers and tidal velocities; $t = 10T$.

sion patterns after one tidal cycle. (Method (e) of Section 4) (Fig. 12).

(d) Tidally-averaged run with Eulerian residual velocities and an isotropic diffusion coefficient of $10.2\ m^2/s$, the average of the values computed with formula (10) (Fig. 13).

Figs. 10 and 11 show a good agreement of method (b) with method (a). Method (b) underestimates the alongshore dispersion somewhat. Detailed output of the computations showed that the peak concentration was higher in run (a).

Method (c) (Fig. 12) underestimates even more the alongshore dispersion. As a result of the high values of the diffusion tensors in the vicinity of the river outlet, there is too much mass retained there. These high values are a result of the irregularity of

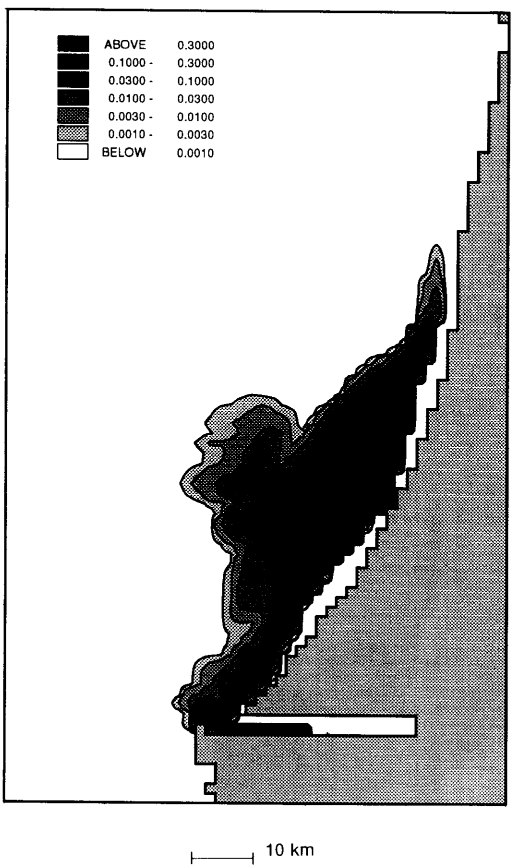

Fig. 11. Dispersion pattern after a point release in point 4. Computation with distributed Lagrangian residual velocities; $t = 10T$.

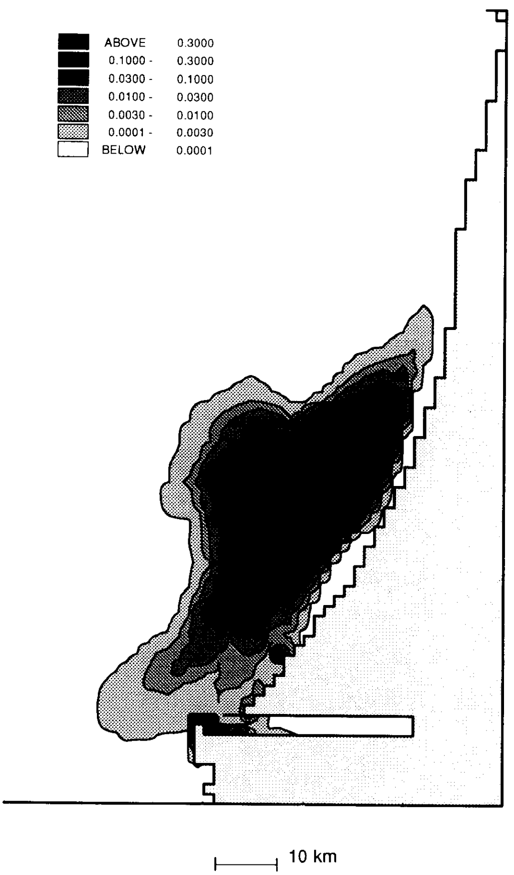

Fig. 12. Dispersion pattern after a point release in point 4. Computation with Lagrangian residual velocities and residual diffusion tensors; $t = 10T$.

the dispersion patterns with important higher order moments, and give an overestimation of the diffusion. When these values are limited in the sense that no tensor determinant has an equivalent diffusion coefficient of more than $50\ m^2/s$, results are improved.

Method (d) (Fig. 13) gives also a large underestimation of the alongshore dispersion. This is caused by the isotropy of the diffusion operator used. The coefficient of $10.2\ m^2/s$ was an average of the entire model area. In the region where the patch spreads out, diffusivities are larger. When a coefficient of $20\ m^2/s$ was taken, the results however did not improve.

It is clear from the results, that the large anisotropy of the dispersion in coastal zones, with

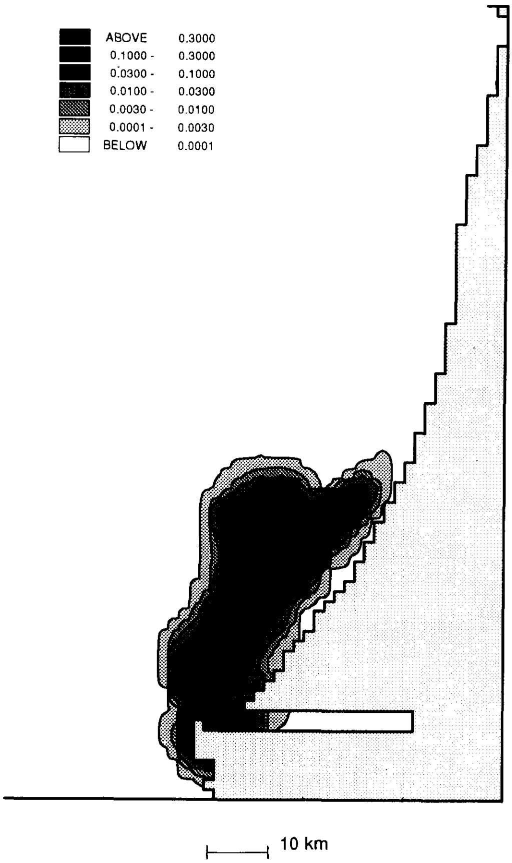

Fig. 13. Dispersion pattern after a point release in point 4. Computation with Eulerian residual velocities and uniform isotropic residual diffusion coefficient of 10.2 m^2/s; $t = 10T$.

alongshore diffusion coefficients of over 100 m^2/s, cannot be modeled by uniform isotropic residual 2-D diffusion operators.

As a method for tidally-averaged advection-diffusion computation (time step 45000 s) in coastal waters, where tidally induced dispersion is very anisotropic and irregular, the use of space-dependent, distributed residual Lagrangian velocities (method (b)), on a grid with mesh size, several times smaller than the tidal excursion, leads to results that are comparable with those of a computation with tidal resolution (time step 1800 s). Addition of distributed diffusion tensors (no results shown) is an improvement of the method, and sometimes necessary, depending on the ratio of tidal excursion and grid mesh size.

The larger computer memory space needed, in comparison with other tidally averaged methods, does not lead to higher computational costs. For the computation of the distributed Lagrangian residuals, tidal velocity fields are needed, including vertical information (two-layer, $2\frac{1}{2}$-D, 3-D).

For a real long-term computation (the residual velocity field of Fig. 4 is not a long-term average), it is of course necessary to have fields of distributed residual transports and diffusion tensors available, for a number of characteristic or significant situations with respect to river run off, wind, tidal amplitude and density structure (stratification, fronts) of the coastal water. Changes of conditions with time scales of a tidal period or more can be included by the choice of the most appropriate tensor field for each time step.

After the initial effort of generating the transport and tensor fields and storing them on disc, the long-term computation takes very little computer time, even on a PC. The tidally averaged transport computation with the Dutch coastal model was 2000× faster than a run with the two-layer hydrodynamical and transport model with tidal resolution.

When it is a too complicated procedure, for an operational model, to store and retrieve many fields with distributed residual displacement vectors and dispersion tensors, it is possible to construct a weighted average according to the probability of the conditions they apply to (see, e.g., Prandle, 1978). The distribution of the residual Lagrangian displacement vector reflects now the probability of the displacement of mass in two-dimensional space.

The result of a long-term computation lacks again a part of the effects of cross products with primes, associated with variations on time scales longer than a tidal period (compare eq. (2)), but can nevertheless be regarded as a long term average. Extensions of the model to suspended sediment transport, but also to processes with time scales of a day and more are rather straightforward, and will make it possible to assess the long term water quality for a large variety of input parameters, weather conditions etc.

7. Acknowledgements

The author thanks Dr. W. de Ruijter, Dr. C. Vreugdenhil and the referees for their valuable comments on the original manuscript.

Mr. G. Bultman wrote a very versatile multifunctional second moment programme and was responsible for most of the transport computations and plots. Miss K. de Jong did a part of the intercomparison of the two-dimensional methods of Krol and Heemink, of Sykes and Henn and of Ridderinkhof.

Appendix A

Vertical mass transport in a two-layer model

In a two-layer system, with known time and space variable upper layer thickness h_1 and lower layer thickness h_2 the horizontal velocities are known as well. The advection through the moving, non horizontal interface between the layers can be computed following:

$$\omega = \frac{\partial h_1}{\partial t} + \nabla^{\mathrm{T}} \int_{z_1}^{z_0} \boldsymbol{u}\, \mathrm{d}z, \qquad h_1 = z_0 - z_1,$$

z_0 is position of surface, z_1 is position of interface (Fig. 14). ω is called "vertical" here for brevity, though it has horizontal components. For the computation of the vertical advective and diffusive mass transports, the following equations have to be solved:

$$\frac{\partial h_1 c_1}{\partial t} - \omega c_i + k_z \frac{c_1 - c_2}{\Delta z} = 0,$$

$$\frac{\partial h_2 c_2}{\partial t} + \omega c_i - k_z \frac{c_1 - c_2}{\Delta z} = 0.$$

$\Delta z = \frac{1}{2}(h_1 + h_2)$, k_z is the vertical diffusive exchange coefficient, c_k is concentration, vertically averaged over layer k, $k = 1, 2$, c_i is concentration at layer interface.

An adapted second moment method is used both for advection and diffusion (Egan and Mahony, 1972; Pederson and Prahm, 1974; de Kok, 1992). The method is positive and of second order. Of the masses $m_1 = h_1 c_1$ and $m_2 = h_2 c_2$ the distance $d_1 = \mu_1 - z_1$ and $d_2 = z_1 - \mu_2$ of the centres to the position of the layer interface, and the vertical variances σ_{zi}^2 are stored. During the horizontal advection step, in which only horizontal first moments and variances are changed, the values of $(d/h)_i$ and $(\sigma_z^2/h^2)_i$, $i = 1, 2$, are kept constant (Fig. 14a). In the vertical advection step, per layer the centre of mass is vertically displaced with its velocity ω_μ, known from linear interpolation between interface and boundary (Fig. 14b). At the boundaries: surface and bottom, $\omega_s = \omega_b = 0$.

Applying eq. (8) in vertical direction and in one dimension one finds for the z-variance:

$$\sigma_z^{2\prime}(t + \Delta t) = \sigma_z^2(t)(1 - \omega\, \Delta t/h_1)^2 + 2k_z\, \Delta t$$

for the upper layer,

$$\sigma_z^{2\prime}(t + \Delta t) = \sigma_z^2(t)(1 + \omega\, \Delta t/h_2)^2 + 2k_z\, \Delta t$$

for the lower layer,

with ω at the interface.

The actual transfer of mass between layers in the model takes place during the redistribution step (Figs. 14c, d). Per layer, the mass is thought to be homogeneously distributed over a distance $R_{zi} = \sqrt{(12\sigma_{zi}^{2\prime})}$ symmetrically around the centre of mass. When $d_i' < \frac{1}{2}R_{zi}$ a part of the mass is present in the other layer. This mass is now assigned to that other layer, and 1st and 2nd horizontal mass moments are subtracted from the mass moments of the donor layer and added to those in the recieving layer. When $(d' + \frac{1}{2}R_z)_i > h_i$, a part of the mass sticks out through surface or bottom. This part is now homogeneously distributed over the area within the layer where mass is present.

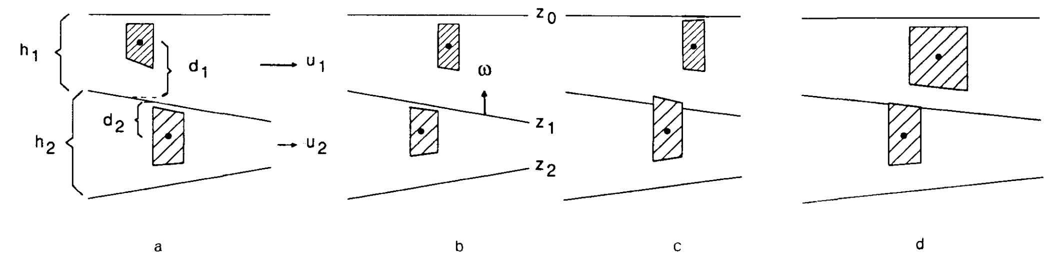

Fig. 14. (a) Initial situation. (b) After horizontal advection step, no change of relative vertical positions. (c) After vertical advection with relative velocity ω, and diffusion. (d) After redistribution.

Vertical 1st and 2nd mass moments are again computed according to:

$$m_i = \int_{z_i}^{z_{i-1}} \int_{\Delta y} \int_{\Delta x} c(x, y, z)\, dx\, dy\, dz,$$

$$m_i \mu_i = \int_{z_i}^{z_{i-1}} \int_{\Delta y} \int_{\Delta x} z c(x, y, z)\, dx\, dy\, dz$$

$$m_i \sigma_i^2 = \int_{z_i}^{z_{i-1}} \int_{\Delta y} \int_{\Delta x} z^2 c(x, y, z)\, dx\, dy\, dz - m_i \mu_i^2.$$

This method assumes discontinuous shape functions (homogeneous distributions) for layer masses and can therefore reproduce vertical concentration profiles associated with discontinous stratification. The position of the discontinuity does not need to coincide with the layer interface.

Appendix B

Relations between $\boldsymbol{K}^*$, d, $\boldsymbol{\Sigma}_0$ and $\boldsymbol{\Sigma}_T$

The accordance of eq. (4) with eq. (2) can be seen as follows.

A point with position $\boldsymbol{x}_0$ at $t=0$, is advected to position $\boldsymbol{x}_0 + \boldsymbol{d}(\boldsymbol{x}_0)$ in a period T. When we assume $\nabla(\boldsymbol{d}(\boldsymbol{x}))^{\mathrm{T}}$ locally constant and $\boldsymbol{d}(0)=0$, then $\boldsymbol{x}_{\mathrm{T}} = \boldsymbol{P}_{\mathrm{r}}^{\mathrm{T}} \boldsymbol{x}_0$, with $\boldsymbol{P}_{\mathrm{r}} = \boldsymbol{I} + \nabla \boldsymbol{d}^{\mathrm{T}}$, $\boldsymbol{d}$ the residual Lagrangian displacement vector in a moving rigid frame.

By diffusion and velocity gradients, an initial point mass has at $t=T$ a covariance matrix given by $2\boldsymbol{K}_{\mathrm{r}} T$, with $\boldsymbol{K}_{\mathrm{r}}$ the residual diffusion coefficient related to initial point masses.

When there is a small cloud of point masses $C(\boldsymbol{x}, 0)$ at $t=0$, and the origin of the moving rigid coordinate system is always in the centre of the cloud, it has at $t=T$ 2nd mass moments:

$$M\boldsymbol{\Sigma}_{\mathrm{T}} = \iint \boldsymbol{x}\boldsymbol{x}^{\mathrm{T}} C(\boldsymbol{x}, T)\, d\boldsymbol{x}$$

$$= \iint (\boldsymbol{P}_{\mathrm{r}}^{\mathrm{T}} \boldsymbol{x}\boldsymbol{x}^{\mathrm{T}} \boldsymbol{P}_{\mathrm{r}} + 2\boldsymbol{K}_{\mathrm{r}} T)\, C(\boldsymbol{x}, 0)\, d\boldsymbol{x}$$

$$= M(\boldsymbol{P}_{\mathrm{r}}^{\mathrm{T}} \boldsymbol{\Sigma}_0 \boldsymbol{P}_{\mathrm{r}} + 2\boldsymbol{K}_{\mathrm{r}} T),$$

with $\boldsymbol{\Sigma}_0$ the initial covariance matrix of the cloud.

$$\boldsymbol{K}_{\mathrm{r}} = (\boldsymbol{\Sigma}^{\mathrm{T}} - \boldsymbol{P}_{\mathrm{r}}^{\mathrm{T}} \boldsymbol{\Sigma}_0 \boldsymbol{P}_{\mathrm{r}})/2T$$

and is assumed constant throughout the cloud.

$$\boldsymbol{K}^* = \boldsymbol{K}_{\mathrm{r}} + (\boldsymbol{\Sigma}_{\mathrm{d}} + \boldsymbol{\Sigma}_{\mathrm{d}}^{\mathrm{T}} \boldsymbol{P}_{\mathrm{r}})/2T, \qquad \boldsymbol{\Sigma}_{\mathrm{d}} = \boldsymbol{\Sigma}_0 \nabla \boldsymbol{d}^{\mathrm{T}}.$$

It has to be noted that $\boldsymbol{K}^*$ is not only spatially varying, but also slightly depends on $\boldsymbol{\Sigma}_0$. $\boldsymbol{K}_{\mathrm{r}}$ depends only on the tidal flow data, and it is therefore more accurate to store $\boldsymbol{d}$ and $\boldsymbol{K}_{\mathrm{r}}$ for all grid points, and to compute $\boldsymbol{K}^*$ at every timestep of the tidally averaged computation, when the current $\boldsymbol{\Sigma}_{\mathrm{to}}$ is known. However, when the most probable values are chosen for the $\boldsymbol{\Sigma}_0$, the use of a fixed $\boldsymbol{K}^*$ is more efficient and leads to only minor errors.

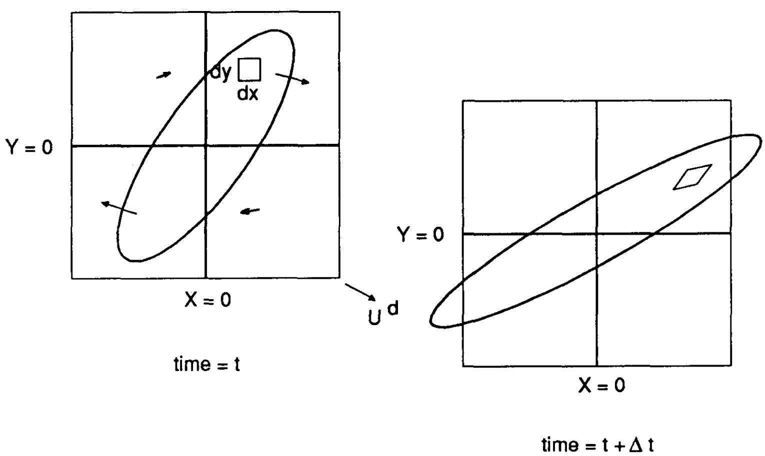

Fig. 15. Moving rigid frame with small cloud that is distorted by differential velocity.

Appendix C

The covariance matrix in vertically averaged differential flow

Let $M = \iint (HC)_{(x,t)}\,\mathrm{d}\boldsymbol{x}$ be the mass and let $M\boldsymbol{\mu}(t) = \iint \boldsymbol{x}(HC)_{(x,t)}\,\mathrm{d}\boldsymbol{x}$ be the first mass moment in Cartesian coordinates of a small cloud that is not necessarily Gaussian. Eq. (7) applies to it. In the rigid frame, that moves with the speed $\boldsymbol{u}^{\mathrm{d}}$ of the centre of mass, which is in the origin of that frame (Fig. 15), $\boldsymbol{\mu} = 0$, and $\boldsymbol{u} = \boldsymbol{u}_{\mathrm{Cartesian}} - \boldsymbol{u}^{\mathrm{d}}$. The 2nd mass moments are:

$$M\sigma_{ij}(t) = \iint x_i x_j (HC)_{(x,t)}\,\mathrm{d}\boldsymbol{x} \tag{18}$$

(compare eq. (3)).

Let $\boldsymbol{x}(t)$ be the position of a column with area $\mathrm{d}\boldsymbol{x}_{(t)} = \mathrm{d}x\,\mathrm{d}y$ at time t. At time $t+\Delta t$, the position is $\boldsymbol{x}(t+\Delta t) = \boldsymbol{P}_x^{\mathrm{T}}\boldsymbol{x}(t)$, and the area is approximated by $\mathrm{d}\boldsymbol{x}_{(t+\Delta t)} = \mathrm{d}\boldsymbol{x}_{(t)} + \nabla^{\mathrm{T}}\boldsymbol{u}\,\Delta t\,\mathrm{d}\boldsymbol{x}_{(t)}$.

$\boldsymbol{P}_x$ is a matrix that can be approximated by $\boldsymbol{P}_x = \boldsymbol{I} + \nabla\boldsymbol{u}^{\mathrm{T}}\,\Delta t$. Again, the 2nd and higher space derivatives and the time derivatives of the velocities are neglected. More accurate approximations of $\boldsymbol{P}_x$ can be derived, if necessary (e.g., Chapman and Dortch, 1991; de Kok, 1993).

From continuity:

$$H(\boldsymbol{x}(t+\Delta t), t+\Delta t)\,\mathrm{d}\boldsymbol{x}_{(t+\Delta t)} = H(\boldsymbol{x}(t), t)\,\mathrm{d}\boldsymbol{x}_{(t)} \tag{20}$$

Without diffusion:

$$C(\boldsymbol{x}(t+\Delta t), t+\Delta t) = C(\boldsymbol{x}(t), t). \tag{21}$$

Using eqs. (18–21), one finds:

$$\begin{aligned}\boldsymbol{\Sigma}^{\mathrm{a}}&(t+\Delta t)\\ &= \iint \boldsymbol{x}(t+\Delta t)\,\boldsymbol{x}^{\mathrm{T}}(t+\Delta t)\,H(\boldsymbol{x}(t), t)\,C(\boldsymbol{x}(t), t)\,\mathrm{d}\boldsymbol{x}_{(t)}\\ &= \boldsymbol{P}_x^{\mathrm{T}}\boldsymbol{\Sigma}(t)\,\boldsymbol{P}_x.\end{aligned}$$

Adding diffusion:

$$\boldsymbol{\Sigma}(t+\Delta t) = \boldsymbol{P}_x^{\mathrm{T}}(t)\,\boldsymbol{\Sigma}(t)\,\boldsymbol{P}_x(t) + 2\boldsymbol{K}(t)\,\Delta t. \tag{22}$$

REFERENCES

Abraham, G. and Gerritsen, H. 1990. Sub-grid transport of matter in two-dimensional tidal flow over an uneven bed. *Continental Shelf Research* **10**, 225–242.

Chapman, R. S. and Dortch, M. S. 1991. 3-D particle tracking for the New-York Bight. In: *Estuarine and coastal modelling* (eds. M. L. Spaulding et al.). New York: ASCE, 26–35.

Cheng, R. T. and Casulli, V. 1982. On Lagrangian residual currents with applications in South San Francisco Bay, California. *Water Resour. Res.* **18**, 1652–1662.

Chikwendu, S. C. and Ojiakor, G. U. 1985. Slow-zone model for longitudinal dispersion in two-dimensional shear flows. *J. Fluid Mech.* **152**, 15–38.

De Kok, J. M. 1992. A finite difference model for computation of near- and far-field transport of suspended matter near a river mouth. *Continental Shelf Research* **12**, 635–642.

De Kok, J. M. 1993. Semi-Lagrangian methods: The Second Moment Method. In: *Numerical methods for advection-diffusion problems* (eds. C. B. Vreugdenhil and B. Koren). Braunschweig, Vieweg.

Dortch, M. S., Chapman, R. S. and Abt, S. R. 1992. Application of three-dimensional Lagrangian residual transport. *J. Hydr. Engineering* **118**, 831–848.

Egan, B. A. and Mahoney, J. R. 1972. Numerical modelling of advection and diffusion of urban area source pollutants. *J. Appl. Met.* **11**, 312–322.

Fischer, H. B., List, E. J., Koh, R. C. Y., Imberger, J. and Brooks, N. H. 1979. *Mixing in inland and coastal waters.* New York. Acad. Press, 483 p.

Heemink, A. W. 1993. Tidally averaged models for dispersion in shallow water. *Water Resour. Res.* **29**, 607–617.

Holly Jr., F. M. and Usseglio-Polatera, J. 1984. Dispersion simulation in two-dimensional tidal flow. *J. Hydr. Engineering* **110**, 905–92.

Krol, M. 1990. *The method of averaging in partial differential equations.* PhD Thesis, University of Utrecht, The Netherlands.

Officer, C. B. and Lynch, D. R. 1981. Dynamics of mixing in estuaries. *Estuarine, coastal and shelf science* **12**, 525–533.

Okubo, A. 1967. The effect of shear in an oscillatory current on horizontal diffusion from an instantaneous source. *Int. J. Oceanol. Limnol.* **1**, 194–204.

Pedersen, L. B. and Prahm, L. P. 1974. A method for numerical solution of the advection equation. *Tellus* **26**, 594–602.

Prandle, D. 1978. Monthly-mean residual flows through the Dover Strait, 1949–1973. *J. Mar. Biol. Ass. U. K.* **58**, 965–973.

Ridderinkhof, H. 1990. *Residual currents and mixing in the Wadden Sea.* PhD Thesis, University of Utrecht, The Netherlands.

De Ruijter, W. P. M., Postma, L. and de Kok, J. M. 1987.

Transport atlas of the southern North Sea. The Hague. Dutch Ministry of Transport, Public Works and Water Management, Tidal Waters Division.

Sykes, R. I. and Henn, D. S. 1992. An improved moment conservation method for the advection-diffusion equation. *J. Appl. Met.* **31**, 112–118.

Uittenbogaard, R. E. 1992. *Large-eddy simulation and long term computation of shallow, free surface flows with 3D-models.* The Hague. Delft Hydraulics/Dutch Ministry of Transport, Public Works and Water Management, Tidal Waters Division.

van Dam, G. C. 1982. Models of dispersion. In: *Pollutant transfer and transport in the sea* (ed. G. Kullenberg). Boca Raton, Florida. CRC Press Inc.

van der Giessen, A., De Ruijter, W. P. M. and Borst, C. 1990. Three-dimensional current structure in the Dutch coastal zone. *Neth. J. Sea. Research* **25**, 45–55.

Zimmerman, J. T. F. 1979. On the Euler-Lagrange transformation and the Stokes drift in the presence of oscillatory and residual currents. *Deep Sea Research* **26**, 505–520.

Zimmerman, J. T. F. 1986. The tidal whirlpool: A review of horizontal dispersion by tidal and residual currents. *Neth. J. Sea Research* **20**, 133–154.